The Astrophysical Journal Letters, 918:L18 (6pp), 2021 September 1 https://doi.org/10.3847/2041-8213/ac1da3

Radio, X-Ray, and Extreme-ultraviolet Observations of Weak Energy Releases in the "Quiet" Sun

R. Ramesh[1], C. Kathiravan[1], N. P. S. Mithun[2], and S. V. Vadawale[2]
[1] Indian Institute of Astrophysics, Koramangala 2nd Block, Bangalore, Karnataka - 560034, India
[2] Physical Research Laboratory, Navrangpura, Ahmedabad, Gujarat – 380009, India
Received 2021 July 8; revised 2021 August 12; accepted 2021 August 13; published 2021 August 31

Abstract

We analyzed ground-based low frequency (<100 MHz) radio spectral and imaging data of the solar corona obtained with the facilities in the Gauribidanur observatory during the same time as the very weak soft X-ray flares (sub-A-class, flux $<10^{-7}$Wm^{-2} in the 1–8 Å wavelength range) from the quiet Sun observed with the X-ray Solar Monitor (XSM) on board Chandrayaan-2 during the recent solar minimum. Nonthermal type I radio burst activity was noticed in close temporal association with the X-ray events. The estimated brightness temperature (T_b) of the bursts at a typical frequency like 80 MHz is $\approx 3 \times 10^5$ K. Extreme-ultraviolet (EUV) observations at 94 Å with the Atmospheric Imaging Assembly (AIA) on board the Solar Dynamics Observatory (SDO) revealed a brightening close to the same location and time as the type I radio bursts. As far as we know reports of simultaneous observations of X-ray and/or EUV counterpart to weak transient radio emission at low frequencies from the quiet Sun in particular are rare. Considering this and the fact that low frequency radio observations are sensitive to weak energy releases in the solar atmosphere, the results indicate that coordinated observations of similar events would be useful to understand transient activities in the quiet Sun.

Unified Astronomy Thesaurus concepts: Quiet sun (1322); Solar radio emission (1522); Solar x-ray flares (1816); Solar corona (1483); Solar activity (1475); Solar flares (1496)

1. Introduction

A variety of small-scale energy releases on the Sun (flaring bright points, active region transient brightenings, coronal jets, etc.) have been studied using X-ray and radio observations. While X-rays are dominated by thermal emission from the coronal plasma, radio observations are sensitive to nonthermal emission also. The observations of low frequency type III radio bursts in association with X-ray bright point flares (Kundu et al. 1980, 1994) clearly indicated that the latter are capable of accelerating particles to nonthermal energies, as well as producing the heated material detected in soft X-rays. The detection of type III bursts together with coronal X-ray jets strengthened the above argument (Aurass et al. 1994; Kundu et al. 1995). These results imply that radio observations are a useful complimentary tool for observing signatures of weak, transient energy releases in the solar atmosphere since the related nonthermal emission can be easily detected (Benz 1995; Mugundhan et al. 2017). Note that counterparts to some of the X-ray transients have been reported at higher radio frequencies also. For example, Gopalswamy et al. (1994), White et al. (1995), and Gary et al. (1997) observed correlated active region transient brightenings in soft X-rays and microwaves. Furthermore, X-ray microflares represent another independent piece of observational evidence for the small-scale energy releases in the solar atmosphere. They were first reported by Lin et al. (1984). The energy involved ($\sim 10^{26}$ erg) is approximately six orders of magnitude lower than the corresponding value for some of the largest solar flares. Sensitive observations with the soft X-ray telescope on board YOHKOH revealed that the microflares are present in the quiet Sun also (Krucker et al. 1997). The study of these microflares is of interest because of their possible bearing on the problems of coronal heating and solar flares (Hudson 1991; Hannah et al. 2011; Benz 2017). Analogous to microflares, Kundu et al. (1986) reported observations of weak nonthermal microbursts in the solar corona at low radio frequencies. Though it was hinted that a common source of energetic particles could be responsible for both the microflares and microbursts, reports of direct association are rare. The microbursts were found to have some characteristics similar to that of the normal type III bursts, but the relationship was inconclusive. Further, the observations reported were at separate individual frequencies unlike typical spectral observations of type III bursts (Kundu et al. 1986; White et al. 1986; Thejappa et al. 1990; Subramanian et al. 1993). Recent spectroscopic imaging observations indicate that the weak nonthermal radio emission at low frequencies is more like type I radio bursts (Sharma et al. 2018; Mondal et al. 2020). However, there were no details about the counterparts to the radio events in other frequency bands of the electromagnetic spectrum. Note that type I bursts represent the smallest discrete releases of observable energy (Bastian et al. 1998). They are considered to be evidence of successive electron accelerations. So, establishing its association with activities in other regions of the solar atmosphere would be useful to understand the acceleration processes of the nonthermal electrons at the sites of elementary/weakest energy releases. In this situation, we report observations of weak type I radio burst emission during the same time as soft X-ray observations of a sub-A class level flare and EUV brightening from the quiet solar corona in the complete absence of active regions and flare/coronal mass ejection (CME) activity.

2. Observations

The radio observations were carried out using the different facilities operated by the Indian Institute of Astrophysics (IIA) in the Gauribidanur Observatory[3] (Ramesh 2011; Ramesh et al.

[3] https://www.iiap.res.in/?q=centers/radio

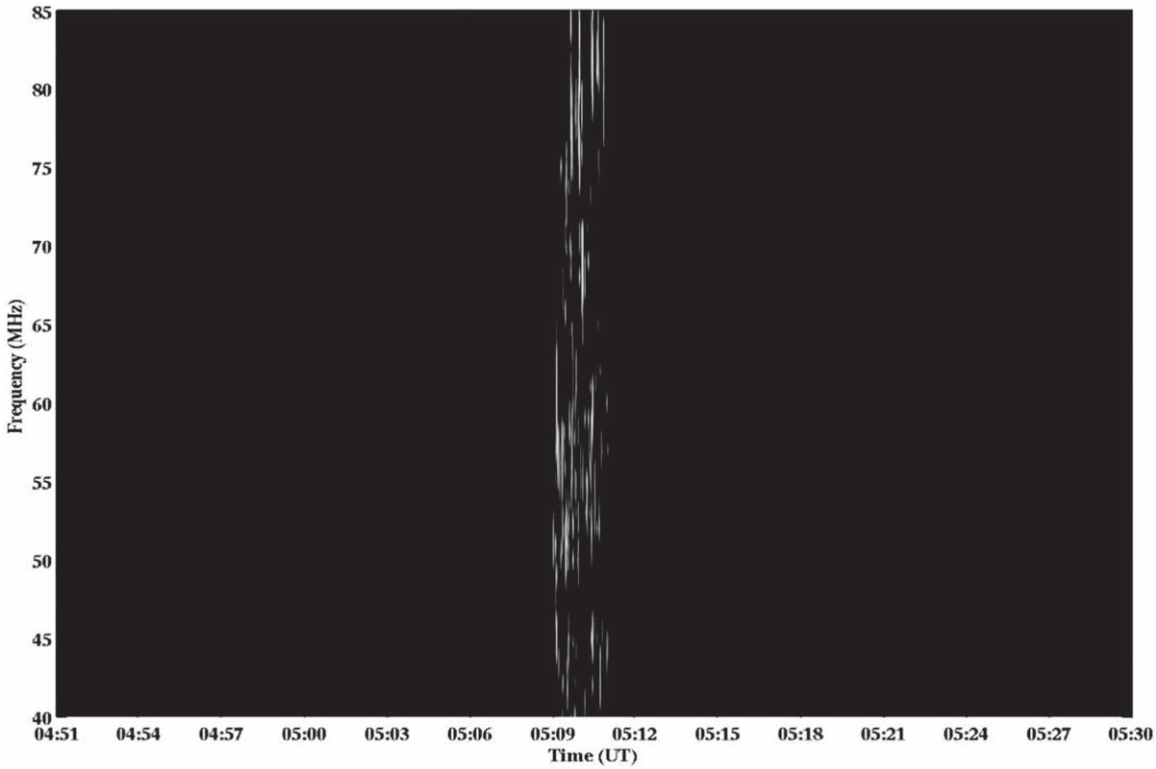

Figure 1. GLOSS dynamic spectrum of the solar radio emission observed on 2020 April 21. The bright emission during the period ≈05:09–05:11 UT correspond to the type I solar radio bursts mentioned in the text.

2014). The radio spectral images were obtained with the Gauribidanur LOw-frequency Solar Spectrograph (GLOSS) in the frequency range 85–40 MHz (Ebenezer et al. 2001, 2007; Kishore et al. 2014; Hariharan et al. 2016b). The GLOSS is a one-dimensional array of eight log-periodic dipole antennas (LPDA) along a north–south baseline. The half-power width of the response pattern of GLOSS around local noon is $\approx 90^\circ \times 6^\circ$ (R.A., R.A.$\times$ decl., decl.) at the highest frequency of operation, i.e., 85 MHz. While the width of the response pattern along R. A. is nearly independent of frequency, its width along the decl. varies inversely with the frequency due to interferometric arrangement of the individual antennas. The observations were carried out with an integration time of ≈1 sec and bandwidth of ≈1 MHz. The minimum detectable flux density is ≈75 Jy (1 Jy $= 10^{-26}$ Wm^{-2} Hz^{-1}) at a typical frequency like 80 MHz. The antenna and the receiver systems were calibrated by carrying out observations in the direction of the Galactic center as described in Kishore et al. (2015). The two-dimensional radio images were obtained with the Gauribidanur RAdioheliograPH (GRAPH) at 80 MHz (Ramesh et al. 1998, 1999a, 2006b). The GRAPH is a T-shaped radio interferometer array of 384 LPDAs. Its angular resolution ("beam" size) for observations close to the zenith is $\approx 5' \times 7'$ (R.A. $\times$ decl.) at the above frequency. The integration time is ≈250 msec and the observing bandwidth is ≈2 MHz. The field of view (FOV) in the GRAPH images is $\approx 2^\circ \times 2^\circ$, and the pixel size is $\approx 14''$. The minimum detectable flux density is ≈2 Jy. The GRAPH data were calibrated using the standard Astronomical Image Processing System (AIPS). The combined use of the imaging and spectral data help us to understand the radio signatures associated with the corresponding solar activity in a better manner (see, e.g., Sasikumar Raja et al. 2014).

Figure 1 shows the GLOSS observations on 2020 April 21 in the time interval 04:51–05:30 UT. The patches of bright emission during the period ≈05:09–05:11 UT are typical of type I or noise storm bursts from the solar corona (see, e.g., Iwai et al. 2013; Mugundhan et al. 2018b). It is widely believed that the bursts are due to plasma radiation at the fundamental plasma frequency (Melrose 1980; Kai et al. 1985). Figure 2 shows the frequency averaged time profile of the dynamic spectrum in Figure 1. The presence of enhanced activity during the interval ≈05:09–05:11 UT could be clearly noticed. It is also similar to the time profiles of groups of type I bursts (see, e.g., Ramesh et al. 2013b; Mugundhan et al. 2016). No Hα and/or GOES soft X-ray flares were reported during the burst interval mentioned above.[4] The Sun was totally free of any active regions[5] and/or CMEs.[6] The overall location of the bursts can be inferred from the GRAPH difference image (obtained by subtracting a pre-event image to clearly identify the weak emission features) in Figure 3 at 80 MHz. The two spatially separated contours marked 1 and 2 correspond to the two maxima (indicated by the same set of numbers) in the time profile of the bursts in Figure 2. The brightness temperature (T_b) of the contours 1 and 2, estimated using the "beam" size of the GRAPH at 80 MHz, are $\approx 3 \times 10^5$ K. The "dots" inside the contours in Figure 3 correspond to the centroids of some of the individual type I bursts (see Figure 4). We located them following the methodology described in Ramesh et al. (2020a). Any ionospheric refraction effects on the radio source positions

[4] https://www.solarmonitor.org/data/2020/04/21/meta/noaa_events_raw_20200421.txt
[5] https://www.solarmonitor.org/?date=20200421
[6] https://cdaw.gsfc.nasa.gov/CME_list/UNIVERSAL/2020_04/univ2020_04.html

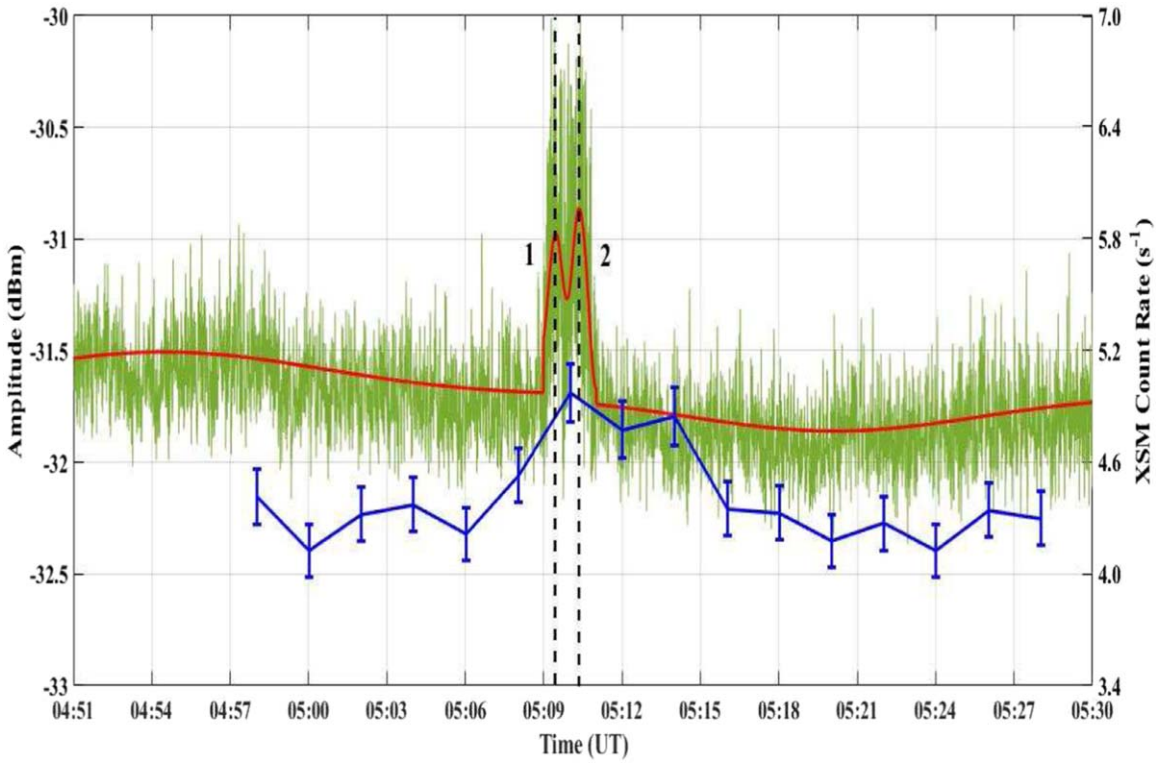

Figure 2. The "green" color plot corresponds to the frequency averaged time profile of the GLOSS dynamic spectrum in Figure 1. Its amplitude values are indicated in the left-hand side ordinate axis. The "red" color line is the fit to the data points. Labels 1 and 2 indicate the epochs of maximum radio emission from regions 1 and 2 in Figure 3, respectively. The "blue" color profile is the light curve of the soft X-ray emission from the Sun close to the same epoch as the radio observations. Its amplitude values are indicated in the right-hand side ordinate axis. The data were obtained with the Chandrayaan-2/XSM (Mithun et al. 2020) in the energy range ≈1–5 keV with a time binning of ≈120 s.

in the present case are expected to be very minimal since the observations were carried out close to the local noon during which time the zenith angle of the Sun is the least. Note that the elevation of Sun on 2020 April 21 during the present radio observations was $\approx 90^{\circ}$. Second, the total duration of the type I radio bursts in the present case is only ≈2 min (see Figures 2 and 4). This is less than the period of ≈20 min over which radio source positions at low frequencies usually change due to ionospheric effects (Stewart & McLean 1982; Mercier 1996).

3. Analysis and Results

Recently, Vadawale et al. (2021) reported observations of quiet-Sun X-ray microflares with the Chandrayaan-2/XSM during the solar minimum 2019–2020 (see, e.g., Ramesh et al. 2020b). Upon inspection we found that some of these flares were observed during the same epoch as the low frequency radio observations of the Sun from Gauribidanur. We considered the X-ray flare observed on 2020 April 21 at ≈05:10 UT (see Figure 2) for the present work since both radio spectral and imaging observations were available. There was also an EUV brightening observed with the SDO/AIA at 94 Å (see Figure 3) around the same time as the type I radio bursts (Figures 1 and 2) and the X-ray flare (Figure 2). The location of the northern radio contour with label "1" in Figure 3 correspond reasonably well with the location of the EUV brightening. The observations of the type I radio bursts over a larger area compared to the EUV brightening could be due to the divergence of the associated field lines (see, e.g., Li et al. 2017). We speculate that the presence of the two spatially separated radio contours 1 and 2 (particularly with the latter located just below the equator in the southern hemisphere) suggests interaction at two different locations between inclined, large magnetic loops with foot points in the same hemisphere, north in the present case (Wild 1968; Simnett 1998). Note that the probability of trans-equatorial loops are expected to be minimal since there were no active regions on the solar disk. Information on the polarization characteristics of the regions 1 and 2 would have helped to verify the above. But observations with the GRAPH in its current configuration are limited to the total intensity mode. We also checked the location of the first sidelobe in the GRAPH "beam," particularly in the north–south direction, to rule out the possibility of any spurious pick-up. It was $\gtrsim 14'$ away from the main lobe. The spacing between contours 1 and 2 in Figure 3 is shorter compared to this. Second, the amplitude of the sidelobe is less by a factor of 20 (≈13 dB). But the strength of sources 1 and 2 are nearly the same.

The peak flux of the XSM flare is $\approx 6 \times 10^{-9}$ Wm^{-2}. It was a very weak event (see Figure 2). The total duration of the event is ≈5 minutes. There appear to be two "peaks" in the flare light curve with a noticeable difference between the corresponding count rates. The type I radio bursts are present only during the initial phase of the X-ray emission, i.e., close to the first of the two "peaks" mentioned above. The total duration of the radio event is smaller (≈2 minutes). Assuming that both the X-ray and radio events are related to a common primary phenomenon, the comparatively shorter duration of the radio event indicates that the electrons responsible for its occurrence are probably thermalized quickly. As a result they cannot travel to larger heights in the corona from where the low frequency radio emission primarily originates (Mondal et al. 2020). The shorter

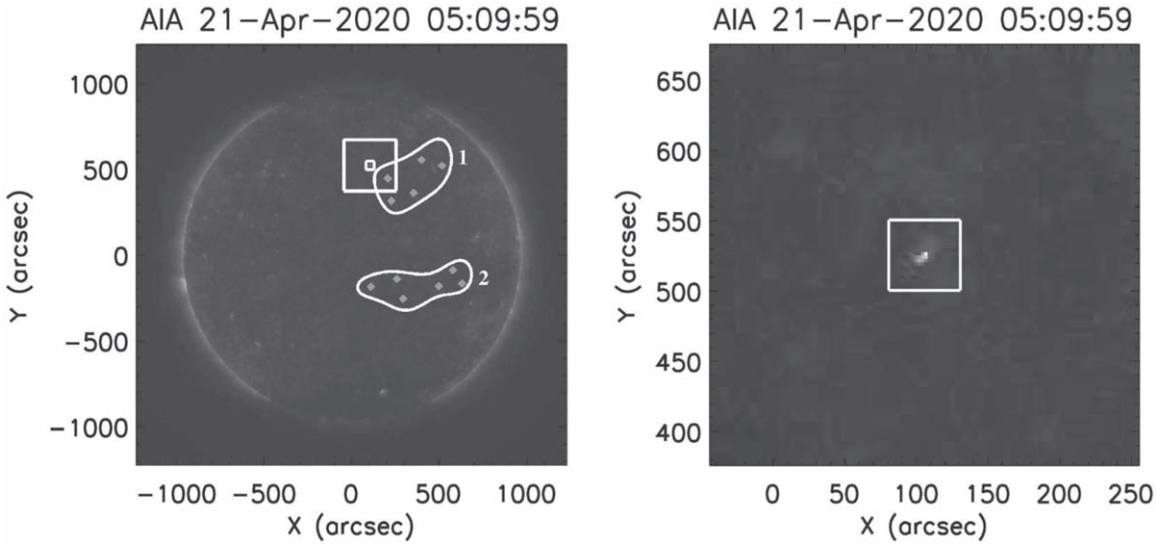

Figure 3. A composite of the GRAPH difference image of the bursts in Figure 1 at 80 MHz and the EUV observations at 94 Å with the SDO/AIA (Lemen et al. 2012) around the same time as the radio and X-ray observations in Figures 1 and 2 on 2020 April 21. The contours labeled 1 and 2 correspond to the GRAPH observations. The background is the EUV image. Solar north is straight up and east is to the left. The bigger and smaller "boxes" in the left panel indicate the region around the EUV brightening and the location of maximum emission, respectively. The "zoomed" version of the same brightening is shown in the right side panel. The peak flux density in the GRAPH observations is ≈241Jy. Its nearly the same for contours 1 and 2, which correspond to the two maxima 1 and 2 in the radio time profile in Figure 2, respectively. The contours shown are at the 80% level. The "dots" inside contours 1 and 2 indicate the centroid locations of the individual type I bursts a–e and f–k in Figure 4, respectively.

duration of the radio bursts could be also due to the emission being nonthermal in nature as compared to the soft X-ray emission (Reid & Vilmer 2017). Nevertheless we independently calculated the associated energy from the radio observations.

The energy associated with a type I burst can be estimated using the relation $E = S\delta t\delta\nu R^2\Omega e^{\tau}$ (Elgaroy 1977). Here S is the flux density of the burst, δt is the duration of the burst, ν is the frequency of observation, $\delta\nu$ is the bandwidth of the burst, R is the Sun–Earth distance, Ω is the solid angle into which the radio waves are emitted, and τ is the optical depth. In the present case, $S \approx 241\,Jy$ (see Figure 3), $\delta t \approx$ 1 s, and $\delta\nu \approx 5$ MHz near 80 MHz (see Figure 1). Assuming $\Omega =$ 0.15 steradians (Steinberg et al. 1974), $\tau \approx 3$ at 80 MHz (Ramesh 2005b), and an efficiency (η) of $\approx 10^{-10}$ for the type I burst emission process (Subramanian & Becker 2004), we find $E \approx 8.1 \times 10^{22}$ erg. This is consistent with the reports that $\sim 10^{21} - 10^{23}$ erg are needed for a single type I burst (James & Subramanian 2018). We also calculated the energy using the relation $E = n_{\rm th}(n/n_{\rm th})VE_{\rm m}$ (see, e.g., Ramesh et al. 2010c). Here $n_{\rm th}$ is the number density of the background thermal electrons, n is the number density of the nonthermal electrons, V is the volume of the burst source, and $E_{\rm m}$ is the mean energy of the individual electrons. In the present case $n_{\rm th} = 7.9 \times 10^7 {\rm cm}^{-3}$ and $E_{\rm m} \approx 5$ keV (Vadawale et al. 2021). Assuming $n/n_{\rm th} = 1.23 \times 10^{-7}$ at 80 MHz (Thejappa & Kundu 1991) and V=$10^{30}{\rm cm}^3$ (corresponding to a density scale height of $\approx 10^{10}$cm in the solar corona), we find $E \approx 7.8 \times 10^{22}$ erg. This is in good agreement with the estimated energy using the observed flux density, duration, bandwidth, etc., of the burst in the present case. We would like to mention here that the noise storm radiative efficiency η mentioned above is typically in the range of $\sim 10^{-6}$–10^{-10}. In the present case both the type I bursts and the associated X-ray emission were short lived. Therefore it is likely that the electron acceleration responsible for the type I bursts were triggered by the same process responsible for the associated X-ray microflare (Crosby et al. 1996). The energy of the latter is typically $\sim 10^{27}$ erg. Reports indicate that for such an energy input, η is expected to be in the range of $\sim 10^{-9}$–10^{-10} (Subramanian & Becker 2004). We assumed $\eta \approx 10^{-10}$ since the observed type I bursts were also weak. The close agreement between the different energy estimates mentioned above is in support of our assumption on the value of η. However, it should be kept in mind that the above calculations will give rise to a lower energy for the type I burst if we assume $\eta > 10^{-10}$. Hence a tighter constraint on the value of η would be better.

Proceeding further, we find that the area enclosed by the contours in Figure 3 is nearly the same as that of the GRAPH "beam" size at 80 MHz mentioned earlier, i.e., $\approx 5' \times 7'$. But results obtained from (i) high angular resolution observations of the solar corona at low radio frequencies during solar eclipses (lunar occultation technique) and (ii) independent long baseline interferometer observations indicate that the "true" size of the individual type I bursts is $\lesssim 15''$ (Ramesh & Ebenezer 2001b; Kathiravan et al. 2011; Ramesh et al. 2012b; Mugundhan et al. 2016, 2018a). There are also reports that the upper limit to the size of a type I burst source is $\approx 14''$ (Melrose 1980). These values are much smaller than the GRAPH "beam" size. Kundu & Gopalswamy (1990), Malik & Mercier (1996), and Willson et al. (1997) had shown earlier that the centroids of type I burst sources are spatially distributed within the associated noise storm emitting region. Type I burst models also predict scattered small-scale sites of energy release (Klein 1995). The dispersion in the centroids of some of the individual type I bursts in the present case (see Figures 3 and 4) is consistent with this. Therefore it is possible that the contours in Figure 3 correspond to an ensemble of type I burst sources, each of size $\approx 14'' \times 14''$. So we calculated the maximum possible total energy of the type I bursts as $E_{\rm t} \approx \frac{5 \times 7 \times 3600 \times 8.1 \times 10^{22}}{14 \times 14} \approx 5.3 \times 10^{25}$ erg. This is in reasonable agreement with the range of

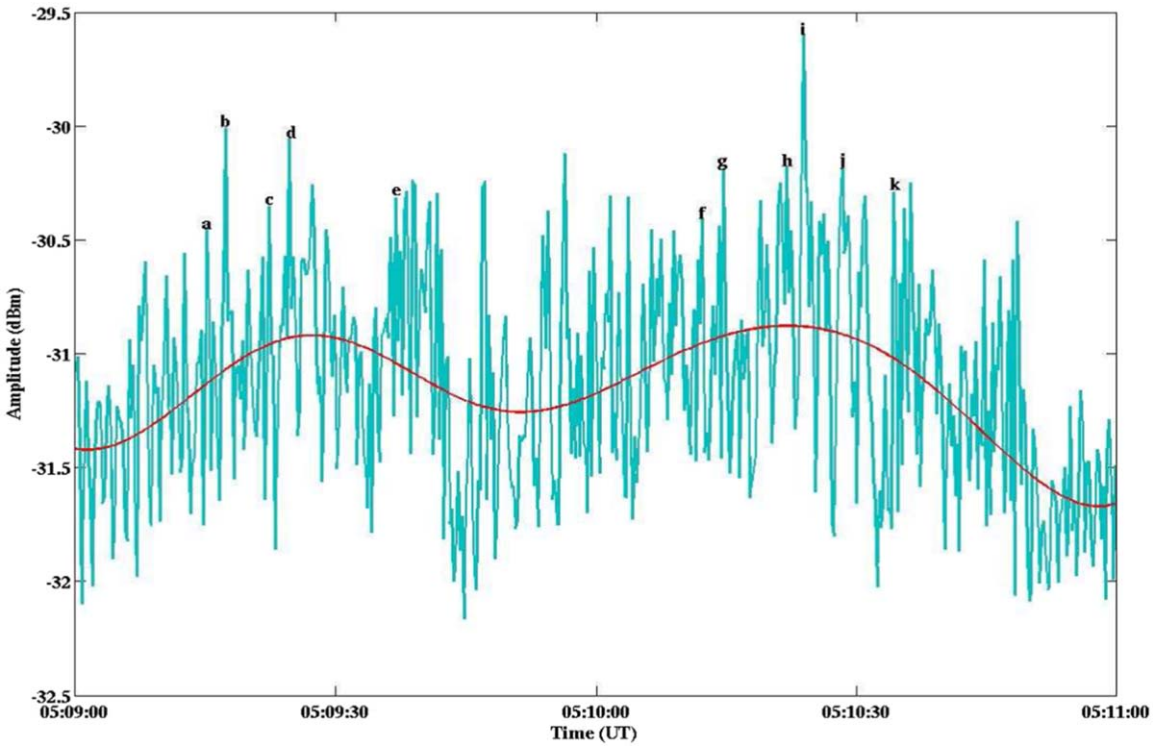

Figure 4. "Zoomed" version of the observations around the maxima in the radio time profile in Figure 2. Labels a–k indicate some of the individual type I bursts.

energies (3×10^{26}–7×10^{27} erg) for the soft X-ray microflares reported by Vadawale et al. (2021) since the authors had mentioned that their estimates represent upper limits. Note that the minimum possible energy of the type I bursts in the present case is $E \approx 8.1 \times 10^{22}$ erg. So our estimates indicate a range of $\approx 10^{22}$–10^{25} erg. Benz & Krucker (2002) had earlier reported EUV flares in the quiet solar corona with energy budget $\approx 10^{24}$–10^{26} erg. Lin (1985) showed that the total energy released into the interplanetary medium in solar electrons above 2 keV is $\approx 10^{25}$–10^{26} erg. The above numbers and arguments confirm that the type I radio bursts are an independent ground-based observational tool to probe weak activity in the quiet regions of the corona also in addition to its known association with sunspot activity (see, e.g., Ramesh & Shanmugha Sundaram 2000b).

4. Summary

We had presented cotemporal/cospatial observations of weak type I radio bursts, X-ray microflare, and EUV brightening from the quiet Sun, which was completely devoid of any active regions. There is close agreement between the energy budgets estimated independently from the radio and X-ray observations. As far as we know, this is the first time such simultaneous observations of transient activity in the quiet Sun have been reported. Considering that type I radio bursts like those described in this work hint that there is activity in the outer layers of the solar corona that is currently inaccessible to observations in X-rays and extreme ultraviolet (EUV), combined investigations of weak energy releases observed at the same time in all the aforementioned domains would be helpful to understand the energies deposited at different levels in the solar corona in addition to the associated mechanisms themselves. For example, Li et al. (2017) showed that magnetic reconnection driven by multiple moving magnetic features (Harvey & Harvey 1973; Bentley et al. 2000) in/near an active region at the photosphere are correlated with EUV brightenings and type I bursts. But there were reports of Hα and X-ray flares during the observing period reported by the above authors. Several active regions were also present. Nevertheless, it would be interesting to explore such moving features in the quiet Sun also (Ramesh et al. 2006a) in order to explain weak energy releases as described in this work.

We express our gratitude to the Gauribidanur observatory staff members for their help in the observations and upkeep of the facilities. M. Rajesh and K. P. Santosh are acknowledged for their assistance to the present work. The SDO/AIA data are courtesy of the NASA/SDO and the AIA science teams. This research has made use of the data from the Solar X-ray Monitor (XSM) on board the Chandrayaan-2 mission of the Indian Space Research Organisation (ISRO), archived at the Indian Space Science Data Centre (ISSDC). XSM was developed by Physical ResearchLaboratory (PRL) with support from various ISRO centers. We thank the referee for kind comments that helped us to describe the results more clearly.

ORCID iDs

R. Ramesh https://orcid.org/0000-0003-2651-0204
S. V. Vadawale https://orcid.org/0000-0002-2050-0913

References

Aurass, H., Klein, K.-L., & Martens, P. C. H. 1994, SoPh, 155, 203
Bastian, T. S., Benz, A. O., & Gary, D. E. 1998, ARA&A, 36, 131
Bentley, R. D., Klein, K.-L., van Driel-Gesztelyi, L., et al. 2000, SoPh, 193, 227
Benz, A. O. 1995, LNP, 444, 1
Benz, A. O. 2017, LRSP, 14, 59
Benz, A. O., & Krucker, S. 2002, ApJ, 568, 413
Crosby, N., Vilmer, N., Lund, N., Klein, K.-L., & Sunyaev, R. 1996, SoPh, 167, 333

Ebenezer, E., Ramesh, R., Subramanian, K. R., Sundara Rajan, M. S., & Sastry, C. V. 2001, A&A, 367, 1112
Ebenezer, E., Subramanian, K. R., Ramesh, R., Sundara Rajan, M. S., & Kathiravan, C. 2007, BASI, 35, 111
Elgaroy, E. Ø. 1977, in Solar Noise Storms (Oxford: Pergamon)
Gary, D. E., Hartl, M. D., & Shimizu, T. 1997, ApJ, 477, 958
Gopalswamy, N., Payne, T. E. W., Schmahl, E. J., et al. 1994, ApJ, 437, 522
Hannah, I. G., Hudson, H. S., Battaglia, M., et al. 2011, SSRv, 159, 263
Hariharan, K., Ramesh, R., Kathiravan, C., Abhilash, H. N., & Rajalingam, M. 2016b, ApJS, 222, 21
Harvey, K., & Harvey, J. 1973, SoPh, 28, 61
Hudson, H. S. 1991, SoPh, 133, 357
Iwai, K., Masuda, S., Miyoshi, Y., et al. 2013, ApJL, 768, L2
James, T., & Subramanian, P. 2018, MNRAS, 479, 1603
Kai, K., Melrose, D. B., & Suzuki, S. 1985, in Solar Radiophysics, 415 ed. D. J. McLean & N. R. Labrum (Cambridge: Cambridge Univ. Press)
Kathiravan, C., Ramesh, R., Indrajit, V. B., & Rajalingam, M. 2011, ApJ, 730, 91
Kishore, P., Kathiravan, C., Ramesh, R., Rajalingam, M., & Indrajit, V. B. 2014, SoPh, 289, 3995
Kishore, P., Ramesh, R., Kathiravan, C., & Rajalingam, M. 2015, SoPh, 290, 2409
Klein, K. L. 1995, LNP, 444, 55
Krucker, S., Benz, A. O., Bastian, T. S., & Acton, L. W. 1997, ApJ, 488, 499
Kundu, M. R., Gergely, T. E., & Golub, L. 1980, ApJL, 236, L87
Kundu, M. R., Gergely, T. E., Szabo, A., Loiacono, R., & White, S. M. 1986, ApJ, 308, 436
Kundu, M. R., & Gopalswamy, N. 1990, SoPh, 129, 133
Kundu, M. R., Raulin, J. P., Nitta, N., et al. 1995, ApJL, 447, L135
Kundu, M. R., Strong, K. T., Pick, M., et al. 1994, ApJL, 427, L59
Lemen, J. R., Title, A. M., Akin, D. J., et al. 2012, SoPh, 275, 17
Li, C. Y., Chen, Y., Wang, B., et al. 2017, SoPh, 292, 82
Lin, R., Schwartz, R. A., Kane, S. R., Pelling, R. M., & Hurley, K. C. 1984, ApJ, 283, 421
Lin, R. P. 1985, SoPh, 100, 537
Malik, R. K., & Mercier, C. 1996, SoPh, 165, 347
Melrose, D. B. 1980, SoPh, 67, 357
Mercier, C. 1996, AnGeo, 14, 42
Mithun, N. P. S., Vadawale, S. V., Sarkar, A., et al. 2020, SoPh, 295, 139
Mondal, S., Oberoi, D., & Mohan, A. 2020, ApJL, 895, L39
Mugundhan, V., Hariharan, K., & Ramesh, R. 2017, SoPh, 292, 155
Mugundhan, V., Ramesh, R., Indrajit, V. B., et al. 2016, ApJ, 831, 154
Mugundhan, V., Ramesh, R., Kathiravan, C., et al. 2018a, ApJL, 855, L8
Mugundhan, V., Ramesh, R., Kathiravan, C., Gireesh, G. V. S., & Hegde, A. 2018b, SoPh, 293, 41
Ramesh, R. 2005b, in IAU Proc. 226, Coronal and Stellar Mass Ejections, ed. K. Dere, J. Wang, & Y. Yan (Cambridge: Cambridge Univ. Press), 83
Ramesh, R. 2011, in ASI Conf. Ser. 2, First Asia-Pacific Solar Physics Meeting, ed. A. R. Choudhuri & D. Banerjee (Bengaluru: BASI), 55
Ramesh, R., & Ebenezer, E. 2001b, ApJL, 558, L141
Ramesh, R., Kathiravan, C., Barve, I. V., Beeharry, G. K., & Rajasekara, G. N. 2010c, ApJL, 719, L41
Ramesh, R., Kathiravan, C., Indrajit, V. B., & Rajalingam, M. 2012b, ApJ, 744, 165
Ramesh, R., Kathiravan, C., Sundara Rajan, M. S., Indrajit Barve, V., & Rajalingam, M. 2014, in ASI Conf. Ser. 13, The Metrewavelength Sky, ed. J. N. Chengalur & Y. Gupta (Bengaluru: BASI), 19
Ramesh, R., Kumari, A., Kathiravan, C., et al. 2020b, GeoRL, 47, e90426
Ramesh, R., Mugundhan, V., & Prabhu, K. 2020a, ApJL, 889, L25
Ramesh, R., Nataraj, H. S., Kathiravan, C., & Sastry, Ch. V. 2006a, ApJ, 648, 707
Ramesh, R., Sasikumar Raja, K., Kathiravan, C., & Satya Narayanan, A. 2013b, ApJ, 762, 89
Ramesh, R., & Shanmugha Sundaram, G. A. 2000b, A&A, 364, 873
Ramesh, R., Subramanian, K. R., & Sastry, C. V. 1999a, A&AS, 139, 179
Ramesh, R., Subramanian, K. R., Sundara Rajan, M. S., & Sastry, C. V. 1998, SoPh, 181, 439
Ramesh, R., Sundara Rajan, M. S., & Sastry, C. V. 2006b, ExA, 21, 31
Reid, H. A. S., & Vilmer, N. 2017, A&A, 597, A77
Sasikumar Raja, K., Ramesh, R., Hariharan, K., Kathiravan, C., & Wang, T. J. 2014, ApJ, 796, 56
Sharma, R., Oberoi, D., & Arjunwadkar, M. 2018, ApJ, 852, 69
Simnett, G. M. 1998, in ASP Conf. Ser. 155, Three-Dimensional Structure of Solar Active Regions, ed. C. E. Alissandrakis & B. Schmieder (San Francisco, CA: ASP), 234
Steinberg, J. L., Caroubalos, C., & Bougeret, J. L. 1974, A&A, 37, 109
Stewart, R. T., & McLean, D. J. 1982, PASA, 4, 386
Subramanian, K. R., Gopalswamy, N., & Sastry, C. V. 1993, SoPh, 143, 301
Subramanian, P., & Becker, P. A. 2004, SoPh, 225, 91
Thejappa, G., & Kundu, M. R. 1991, SoPh, 132, 173
Thejappa, G., Kundu, M. R., & Gopalswamy, N. 1990, SoPh, 127, 165
Vadawale, S. V., Mithun, N. P. S., Mondal, B., et al. 2021, ApJL, 912, L13
White, S. M., Kundu, M. R., Shimizu, T., Shibasaki, K., & Enome, S. 1995, ApJ, 450, 435
White, S. M., Kundu, M. R., & Szabo, A. 1986, SoPh, 107, 135
Wild, J. P. 1968, PASA, 1, 137
Willson, R. F., Kile, J. N., & Rothberg, B. 1997, SoPh, 170, 299